Mesoscale Modeling of the Atmosphere over Antarctic Sea Ice: A Late-Autumn Case Study

TERESA VALKONEN

Department of Physics, University of Helsinki, Helsinki, Finland

TIMO VIHMA

Finnish Meteorological Institute, Helsinki, Finland

MARTIN DOBLE

Department of Applied Mathematics and Theoretical Physics, University of Cambridge, Cambridge, United Kingdom

(Manuscript received 25 April 2007, in final form 13 July 2007)

ABSTRACT

Atmospheric flow over Antarctic sea ice was simulated applying a polar version of the fifth-generation Pennsylvania State University–National Center for Atmospheric Research Mesoscale Model (Polar MM5). The simulation period in late autumn lasted for 48 h, starting as northerly warm airflow over the Weddell Sea ice cover and turning to a southwesterly cold-air outbreak. The model results were validated against atmospheric pressure and wind and air temperature observations made by five buoys drifting with the sea ice. Four different satellite-derived sea ice concentration datasets were applied to provide lower boundary conditions for Polar MM5. During the period of the cold-air outbreak, the modeled air temperatures were highly sensitive to the sea ice concentration: the largest differences in the modeled 2-m air temperature reached 13°C. The experiments applying sea ice concentration data based on the bootstrap and Arctic Radiation and Turbulence Interaction Study (ARTIST) algorithms yielded the best agreement with observations. The cumulative fetch over open water correlated with the bias of the modeled air temperature. The sea ice concentration data affected the simulated air temperature in the lower atmospheric boundary layer, but above it the temperature and wind fields were more strongly controlled by the boundary layer scheme applied in Polar MM5. Analysis nudging applying four-dimensional data assimilation had a positive effect on the pressure and wind fields but negative or no effect on the air temperature fields. The results suggest that applying a sea ice model to update sea ice fields frequently throughout atmospheric model simulations will likely lead to important improvements in forecasts.

1. Introduction

The Antarctic sea ice zone covers approximately 19×10^6 km^2 in winter and 3.5×10^6 km^2 in summer (Parkinson 2004). In situ observations of the atmosphere over this vast area have been rare, restricted to ship observations (mostly summertime; Andreas 1985; Wendler et al. 2005), wind and temperature measurements from drifting buoys (Kottmeier and Sellman 1996), and detailed boundary layer observations from two drifting ice stations, in 1992 (Andreas et al. 2000, 2004) and 2004–05 (Bareiss 2008). Data allowing the resolution of mesoscale variations in the atmosphere have been practically absent.

A few meteorological modeling studies have addressed the Antarctic sea ice zone. Bennet and Hunkins (1986) applied a two-dimensional model to simulate warm-air advection over the Weddell Sea ice cover, but only observations from a moving ship were available to validate the results. Renfrew and King (2000) developed and validated a mixed-layer slab model for convective boundary layer over polynyas in the Antarctic sea ice zone. This model was utilized in surface heat budget studies by Renfrew et al. (2002). Idealized model experiments without detailed validation against observations have been also been made (Simmonds and

Corresponding author address: Dr. Timo Vihma, Finnish Meteorological Institute, P.O. Box 503, 00101 Helsinki, Finland.
E-mail: timo.vihma@fmi.fi

DOI: 10.1175/2007MWR2242.1

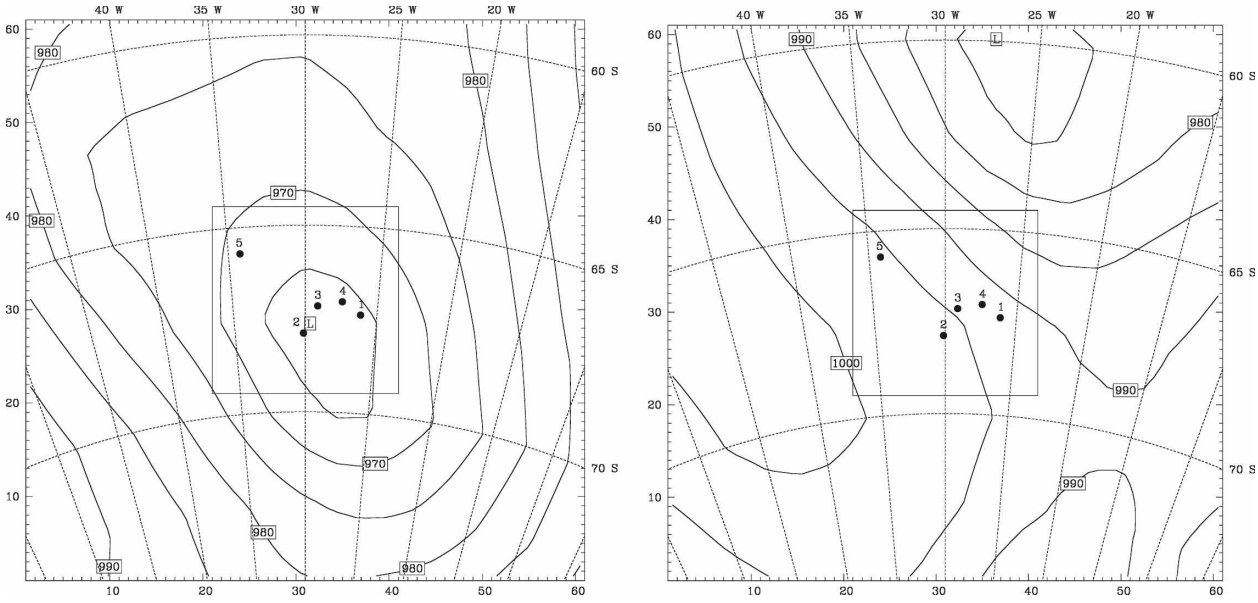

FIG. 1. Mean sea level pressure fields in the Weddell Sea at (left) 1200 UTC 24 May and (right) 1200 UTC 25 May, on the basis of ERA-40. The five dots in the inner model domain (square) represent the drifting buoys.

Budd 1991; Watkins and Simmonds 1995; Dare and Atkinson 1999; Birnbaum 2003). In several Antarctic modeling experiments, the model domains have also included sea ice areas, but the focus has been on coastal features (Parish and Wendler 1991; Guo et al. 2003; Bromwich et al. 2005; Adams 2005; Parish and Walker 2006).

From the point of view of the atmospheric boundary layer (ABL), sea ice is a special type of surface. A sea ice cover consists of ice floes of varying thickness and is broken by cracks, leads, and polynyas. Surface conditions are controlled by closely interacting dynamic and thermodynamic processes. The surface roughness of ice-covered seas is more homogeneous than most continental terrains, but variations in this roughness are important for the wind forcing of sea ice drift (Lüpkes and Birnbaum 2005). On the other hand, over ice-covered seas in winter the surface temperature distribution is extremely heterogeneous. Open-water areas have a surface temperature practically at the freezing point of seawater (approximately -1.8°C), while the surface temperature of thick, snow-covered ice floes in the Antarctic sea ice zone can be less than -30°C. Thin new ice has some intermediate surface temperature. Such spatial variations are among the largest surface temperature step changes found on earth. Several studies have addressed the effects of leads and polynyas on the ABL, though these have been mostly based on Arctic observations or numerical modeling (Andreas et al. 1979; Vihma 1995; Alam and Curry 1997; Pinto et al. 2003; Mauritsen et al. 2005; Inoue et al. 2005). The observations have included measurements of turbulent fluxes over and downwind of individual leads, but estimation of the regional effects of leads on surface exchange processes in the Antarctic sea ice zone is made difficult by the lack of accurate information on sea ice concentration (Vihma et al. 2002). Satellite-derived sea ice concentration exhibit significant variations between algorithms, particularly in conditions of a high (>90%) ice concentration.

In the ice edge zone, the importance of leads on the ABL varies with the synoptic-scale flow conditions (Vihma and Brümmer 2002). During warm-air advection from the open sea to sea ice, the lead effects are weaker as the ABL is approximately in thermal balance with the open water. During off-ice flows, lead effects are stronger as the ABL is usually roughly in balance with the surface temperature of the sea ice and this also applies in the interior of the ice pack. In winter the sum of sensible and latent heat fluxes can reach several hundred watts per square meter (Andreas and Cash 1999). In the Southern Ocean, the mean characteristics of the air–sea interaction also depend on whether the climatological circumpolar trough locates to the north or south of the sea ice edge (Simmonds et al. 2005).

In this study, we examine a 2-day period, which started as a northerly warm-air advection over the Weddell Sea ice cover before turning to a cold, southerly, and later southwesterly, off-ice flow. The pressure fields during the northerly and southerly flow are shown in Fig. 1. This case was selected because the rapid change in the large-scale flow conditions yielded

dramatic changes in the turbulent surface fluxes and ABL stratification, and hence the case presents a great challenge for mesoscale modeling. The atmospheric pressure, air temperature, and wind were recorded by five buoys drifting approximately 100 km apart in the northern part of the sea ice zone. We apply a polar version of the fifth-generation Pennsylvania State University–National Center for Atmospheric Research (NCAR) Mesoscale Model (Polar MM5) to simulate the flow over the fractured sea ice cover, and model results are validated against buoy data. Four different sea ice concentration datasets are applied as lower boundary conditions for the model. Our main objective is to improve understanding of the ABL sensitivity to sea ice concentration. We also examine the ABL scheme and analysis nudging and their effects on model results.

2. Observations

Six drifting buoys were deployed in the Weddell Sea in April 2000 as a part of the Short Timescale Motion of Pancake Ice (STiMPI) project (Doble et al. 2003). The buoys were initially deployed between pancakes at the limit of the zone. By 3 May the pancakes had consolidated into the more familiar pack ice and the buoys were embedded within this, tracking its drift (Doble and Wadhams 2006). Each buoy measured the atmospheric pressure, air temperature, wind speed, and wind direction at the height of 1 m ASL. These lower-than-normal heights for meteorological measurements were due to stability requirements in the harsh conditions that the buoys were expected to experience. The data were recorded once an hour, and the buoy location was measured by GPS every 20 min. Data were transmitted using Argos and Orbcomm satellite systems.

Based on the temperature and wind data, a 48-h period starting from 1800 UTC 23 May 2000 was chosen for model simulation. One of the buoys was no longer operating at that time so data from five buoys were used in this study. During the period, one buoy was located approximately 200 km and the rest 300–400 km from the ice edge. Prior to and during the first half of the simulation period, the measured air temperature was close to the freezing point of seawater, but then rapidly dropped. The temperature drop was associated with a transient low pressure system: the wind direction changed from northeast in the beginning to southwest at the end of the simulation period. During the 48-h simulation period the drift of the pack ice was rather limited (Table 1) and we therefore use the buoy mean locations.

TABLE 1. Mean locations of the buoys, together with the average distance d and maximum distance d_{max} from the mean location during the simulation period. The dml numbers refer to the coding in Doble and Wadhams (2006).

Buoy	Mean location	d (km)	d_{max} (km)
1 (dml8)	67.35°S, 26.14°W	7.0	12.4
2 (dml9)	67.88°S, 30.13°W	12.3	23.7
3 (dml5)	67.15°S, 29.14°W	10.2	22.1
4 (dml7)	67.02°S, 27.45°W	7.0	18.6
5 (dml6)	65.70°S, 34.24°W	9.5	20.1

3. Model

Model simulations were made using the Polar MM5, a limited-area, nonhydrostatic, terrain-following sigma-coordinate model designed to simulate or predict mesoscale and regional-scale atmospheric circulation. The full description of the standard model system is presented by Grell et al. (1994).

Polar MM5 was developed at The Ohio State University, optimizing the standard MM5 for the environment of polar ice sheets. Modifications are described by Cassano et al. (2001) and Bromwich et al. (2001). For the present study, the most important ones are the addition of fractional sea ice surface type and improved calculation of heat transfer through snow and ice surfaces. For fractional sea ice, turbulent heat fluxes are calculated using the flux aggregation, or mosaic, method (Claussen 1990): fluxes are calculated separately for ice and water fractions and area-averaged before interacting with the atmosphere. Heat conduction in snow and ice is predicted with an eight-layer model where the thermal properties of snow and ice are specified by Yen (1981). The sea ice thickness in Polar MM5 depends on the hemisphere and, in the Northern Hemisphere, ice concentration, but a constant value of 0.23 m is applied in the Southern Ocean. Although this must be an underestimation in general, the value is realistic for our study region around 67°S in late May: the thin pancakes had consolidated into pack ice only 20 days prior to the simulation period. Albedo is determined to be 0.80 for a terrestrial ice sheet, 0.70 for sea ice, and 0.15 for open water. The aerodynamic roughness length z_0 is set as 1×10^{-3} m for sea ice and 1×10^{-4} m for ice sheet, and for the open water calculated from the Charnock relation with a minimum of 1×10^{-4} m.

The MM5 model system includes a large number of available physics options. In this study, longwave and shortwave radiation transfer through the atmosphere is parameterized with the NCAR Community Climate Model, version 2, (CCM2) radiation scheme (Hack et al. 1993). Large-scale cloud and precipitation processes

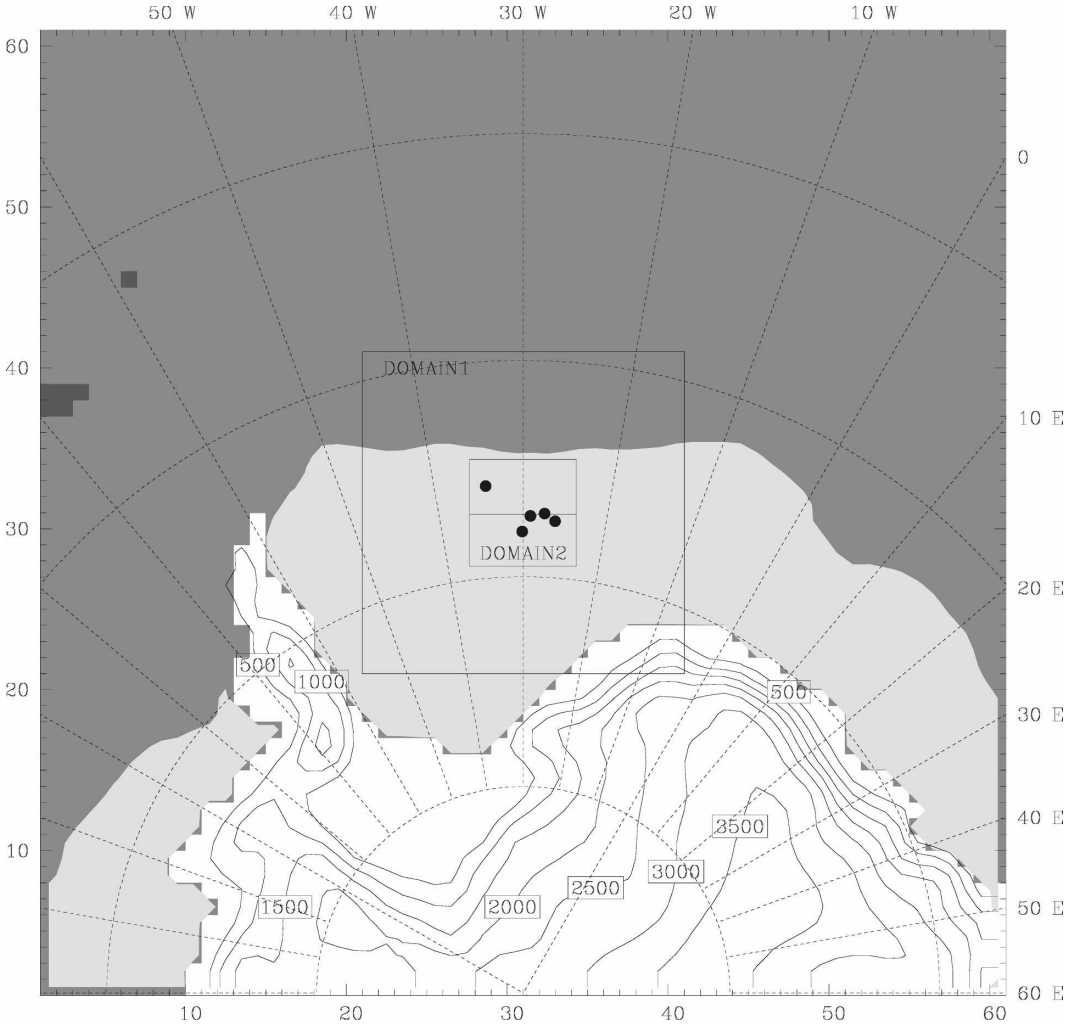

FIG. 2. Domains of Polar MM5. The ice sheet is marked with white color, sea ice (concentrations higher than 50%) with light gray, and open sea with medium gray. The black horizontal line in the middle of domain 2 denotes the location of cross sections shown in Fig. 10.

are parameterized applying Reisner 1 microphysics scheme (Reisner et al. 1998) and subgrid-scale clouds applying the Grell cumulus parameterization (Grell et al. 1994). The atmospheric boundary layer parameterization schemes are introduced later.

Polar MM5 has been successfully applied to Antarctica. Guo et al. (2003) evaluated a complete annual cycle of 72-h simulations at 60-km resolution over Antarctica and found that Polar MM5 captures both the large- and regional-scale circulation features with generally small bias in the modeled variables. Monaghan et al. (2003) demonstrated the model's superiority in the Antarctic compared to the standard version of MM5. Bromwich et al. (2005) evaluated Polar MM5 focusing on synoptic-scale events at certain stations applying domains with horizontal resolutions ranging from 3.3 to 30 km, and Monaghan et al. (2005) analyzed the twice-daily forecasts from the 3.3-km resolution domain to study the climate of the McMurdo region. These studies focused on continental or coastal areas, whereas our interest lies in the sea ice zone.

4. Simulation strategy

a. Domains, initial conditions, and lateral boundary conditions

The model system in this study consists of two polar stereographic domains at the horizontal resolution of 9 and 27 km (Fig. 2). Both domains have 61 × 61 grid points in horizontal directions and they are centered at 67°S, 30°W. A total of 39 vertical sigma levels are used, of which 24 are in the lowest 1000 m of the atmosphere,

and the lowest model level is located at a nominal height of 2 m. The model top is set at the 100-hPa pressure level. The simulations performed are summarized in Table 2.

The Polar MM5 model was initialized by the European Centre for Medium-Range Weather Forecasts (ECMWF) 40-yr reanalysis (ERA-40; Uppala et al. 2005), which has a horizontal resolution of 1.125°. The 6-hourly analyses were used to provide lateral boundary conditions during the simulation. They completely specify the values at the boundary of outer domain. The next four Polar MM5 grid points inward from that boundary were relaxed toward the boundary values with a relaxation constant that decreases linearly away from the boundaries. Between the MM5 domains, there was a two-way interaction, where the inner domain takes boundary information from the outer domain and runs three time steps for each parent step before feeding back information to the outer domain on the coincident interior points (Dudhia et al. 2005). We applied time steps of 6 and 18 s. Utilization of the ECMWF model products for boundary conditions of Polar MM5 was recommended by Bromwich et al. (2003).

Four-dimensional data assimilation (FDDA), or nudging, allows the model to be run with forcing terms that nudge it toward the observations or an analysis (Dudhia et al. 2005). We employ this method using the ERA-40 reanalysis. The reanalysis is based on all available observations, and can be considered as an indirect source of observational data. The benefit of FDDA is that the analyses keep the model closer to realistic conditions and compensate for errors and gaps in the initial analysis and deficiencies in the model physics, while the model equations assure a dynamical consistency. Newtonian relaxation terms are added to the prognostic equations for wind, temperature, and water vapor three-dimensionally in every grid point in the outer domain but not at the surface. These terms relax the model value toward the given analysis. The model linearly interpolates the analyses in time to determine the value toward which the model relaxes its solution (Dudhia et al. 2005). The relaxation terms represent, however, nonphysical terms in the prognostic equations, and Dudhia et al. (2005) do not recommend their use in scientific case studies. To better understand the issue, we run the experiments both with and without nudging (Table 2).

TABLE 2. Model experiments.

Expt No.	Nudging	Sea ice concentration data
1	No	ERA-40
2	No	NASA Team
3	No	Bootstrap
4	No	ARTIST
5	No	ERA-40*
6	Yes	ERA-40
7	Yes	NASA Team
8	Yes	Bootstrap
9	Yes	ARTIST

* MRW ABL scheme applied instead of the Eta scheme.

b. *Lower boundary conditions*

At the lower boundary of the model, the terrain elevation is specified by the Global 30 arc s Elevation Dataset (GTOPO30) from the U.S. Geological Survey (USGS) and the land use by 25-category data of USGS. Our domains, however, only include open sea, sea ice, and the Antarctic continental ice sheet. We applied four different datasets for sea ice concentration: ERA-40, National Aeronautics and Space Administration (NASA) Team, bootstrap, and Arctic Radiation and Turbulence Interaction Study (ARTIST) (Table 2). All of them are based on satellite measurements from the Special Sensor Microwave Imager (SSM/I). In ERA-40, the sea ice concentration is based on the weekly National Centers for Environmental Prediction (NCEP) two-dimensional variational data assimilation (2DVAR) data (Fiorino 2007). In 2000, the data were based on daily SSM/I satellite observations provided by Bristol University. Daily values of sea ice concentration were interpolated from weekly values. The original resolution of ERA-40 dataset is 1.125°, which is approximately 130 km in the meridional and 50 km in the zonal direction in the domain area.

We applied two datasets from the National Snow and Ice Data Center (NSIDC): the NASA Team algorithm (Swift and Cavalieri 1985; Cavalieri et al. 2006) and the bootstrap algorithm (Comiso 1986, 2006; Comiso and Sullivan 1986), which both have a spatial resolution of 25 km. We also utilized the sea ice concentration algorithm developed in ARTIST (Kaleschke et al. 2001; Kern et al. 2003). Resolution of the ARTIST sea ice dataset is 12.5 km, which is an order of magnitude better than that of ERA-40. The NASA Team, the bootstrap, and the ARTIST sea ice datasets are produced daily, but as changes were minor we kept the sea ice concentration constant over the 48-h simulation period. In many cases this would not be a good practice, as cyclones can generate rapid changes in ice motion and concentration (Watkins and Simmonds 1998; Dierer et al. 2005; Wassermann et al. 2006).

The four datasets of sea ice concentration in domain 1 are shown in Fig. 3. The ERA-40 sea ice concentration field does not include small-scale features, and the ice margin zone is wider than in any other dataset. The

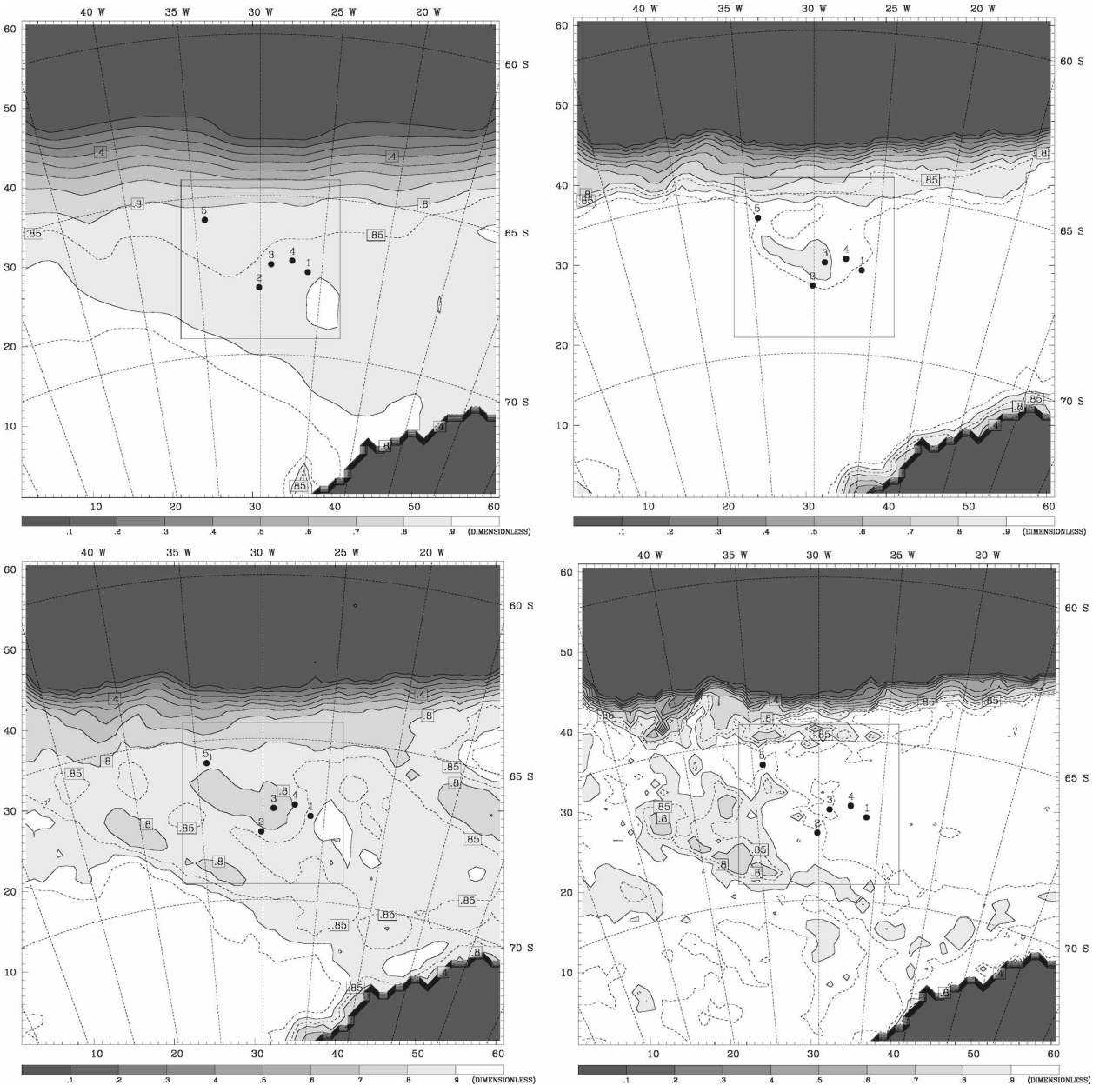

FIG. 3. Sea ice concentration in domain 1 based on four datasets: (top left) ERA-40, (top right) bootstrap, (bottom left) NASA Team, and (bottom right) ARTIST. The interval of solid contour lines is 10%, and the 85% and 95% concentration contours are marked with dashed lines.

NASA Team results have the lowest and the bootstrap the highest concentration values in the study area. The ARTIST sea ice concentration includes small-scale variations, and the sea ice margin is clearly narrower than in the other datasets.

Although the ERA-40 sea ice concentration data are not particularly detailed relative to the other three datasets, they are often used in modeling studies and thus we include them here. We chose the ERA-40 sea ice data over that from the ECMWF operational analysis because the ERA-40 data are more realistic. During our study period in 2000, the sea ice concentration in the ECMWF operational analyses was set to either 0 or 1 for each grid cell, which may generate large errors in surface fluxes and near-surface temperature and humidity.

c. *Two ABL schemes*

The ABL was parameterized applying two schemes. Most of the simulations employed the 1.5-order turbu-

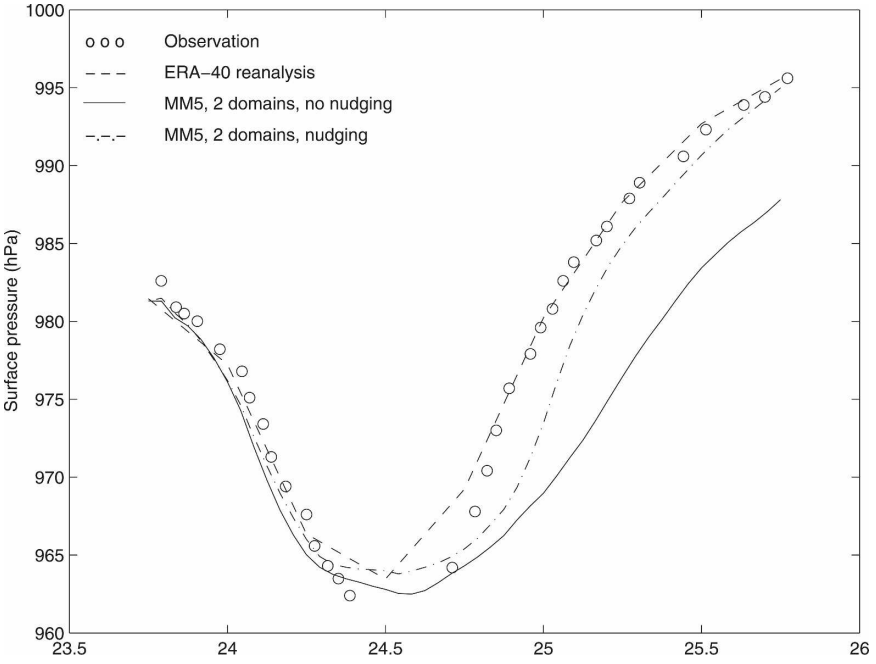

FIG. 4. Time series of atmospheric pressure at buoy 4 in experiments 1, 6, 10, and 12 applying ERA-40 sea ice concentration.

lence closure parameterization used in the NCEP Eta Model (Janjic 1994). A sensitivity test was made applying the boundary layer parameterization from the Medium-Range Forecast Model (MRF) of NCEP (Hong and Pan 1996). This parameterization was used in experiment 5, without nudging and applying sea ice concentration from ERA-40 (Table 2). The MRF scheme is based on the first-order closure and nonlocal turbulent transport with countergradient fluxes in convective cases.

5. Results

Several aspects have to be kept in mind when comparing the atmospheric pressure, air temperature, and wind fields based on ERA-40 and MM5 simulations. First of all, ERA-40 is based on utilization of all available observations: the buoy pressure data were directly assimilated into ERA-40 and the air temperatures were affected by assimilation of satellite data (Uppala et al. 2005). In addition, surface observations and rawinsonde soundings, above all at the Antarctic Peninsula and the Queen Maud Land, have improved the quality of ERA-40 in our study region. On the other hand, in the MM5 experiments we did not assimilate direct observations. The MM5 simulations were only indirectly affected by observations, via the ERA-40-based initialization, the 6-hourly updated boundary conditions, and, in experiments 6–9, the analysis nudging. Hence, on the basis of this study we cannot directly compare the performance of the ECWMF model and MM5. Instead, we can compare the various MM5 simulations against each other.

a. Atmospheric pressure

Figure 4 presents the time series of the observed and modeled atmospheric pressure at buoy 4 (as an example; the results were qualitatively similar for all buoys). The pressure fields based on experiments applying FDDA were better than those without FDDA. The FDDA, however, caused some disturbances in the temperature and wind fields, and we therefore show results of the air temperature and wind both from experiments with and without FDDA.

b. Air temperature and wind

Time series of air temperature are shown in Fig. 5, and the bias and RMS error of each experiment, averaged over the 48-h period and the five buoys, are presented in Table 3. Experiments applying bootstrap and ARTIST sea ice concentrations have the smallest bias and RMS errors, while NASA Team results have the highest bias and RMS errors of experiments applying the Eta ABL scheme. The experiment with ERA-40 sea ice concentration and MRF ABL scheme has, however, even larger bias and RMS errors. The biases are

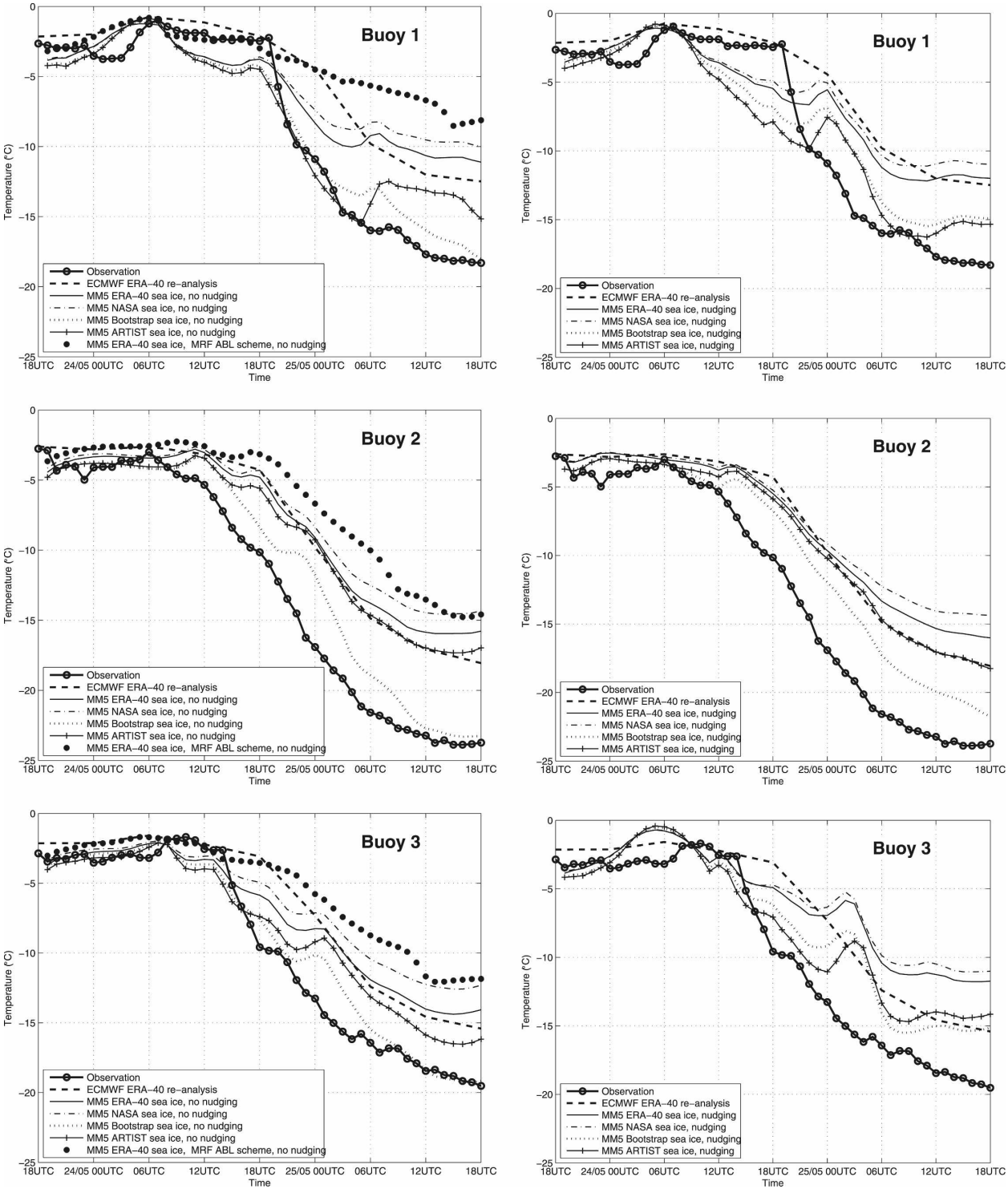

FIG. 5. Time series of air temperature; (left) experiments without nudging and (right) experiments with nudging.

generally positive (Table 3), and the bootstrap and ARTIST are the only algorithms that occasionally yield too-cold air temperatures also during the period of southerly winds (Fig. 5). In conditions of observed air temperature exceeding −5°C (during northerly winds), the best results were obtained in experiment 1 (ERA-40 ice concentration), but the differences between the experiments were minor and all biases had magnitudes

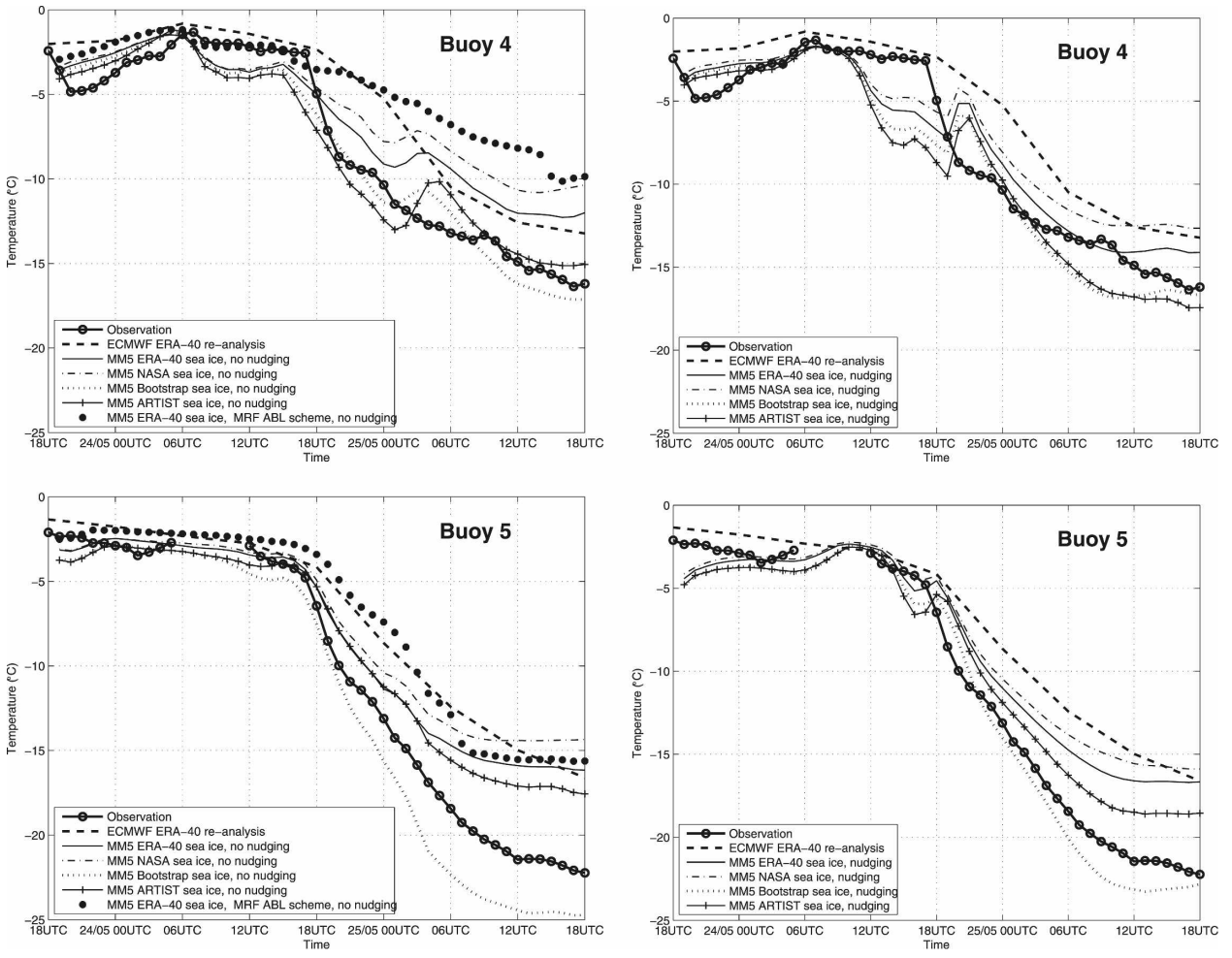

FIG. 5. (*Continued*)

less than 0.9°C and all RMS errors were less than 1.9°C. The errors started to increase immediately after the drop in the observed air temperature (Fig. 5). With the observed temperature less than −5°C, the biases ranged from 0.3° (experiment 3, bootstrap) to 7.2°C (experiment 5, MRF) and the RMS errors from 2.0° (experiment 3) to 7.3°C (experiment 5). Also during the cold period, the ARTIST algorithm yielded the second-best results after the bootstrap algorithm.

In Fig. 6 we show the observed and modeled temperature difference between buoys 4 and 2, which were located an average of 149 km from each other and represented the warmest (4) and coldest (2) of the buoys. It is worth noting that the MM5 results are clearly better without nudging. The best results are achieved in experiment 3 (bootstrap ice concentration, without nudging), and are slightly better than the ERA-40 results. The ARTIST sea ice concentration gave the poor-

TABLE 3. Bias and RMSE of the simulated air temperature.

Simulation	No nudging		Nudging	
	Bias (°C)	RMSE (°C)	Bias (°C)	RMSE (°C)
ECMWF ERA-40	3.1	3.9		
MM5 ERA-40 sea ice	2.6	3.7	2.6	3.8
MM5 NASA Team sea ice	3.2	4.5	3.1	4.3
MM5 bootstrap sea ice	−0.0	1.7	0.7	2.4
MM5 ARTIST sea ice	1.4	2.7	1.2	2.9
MM5 ERA-40 sea ice, MRF ABL scheme	4.3	5.5	No experiment	No experiment

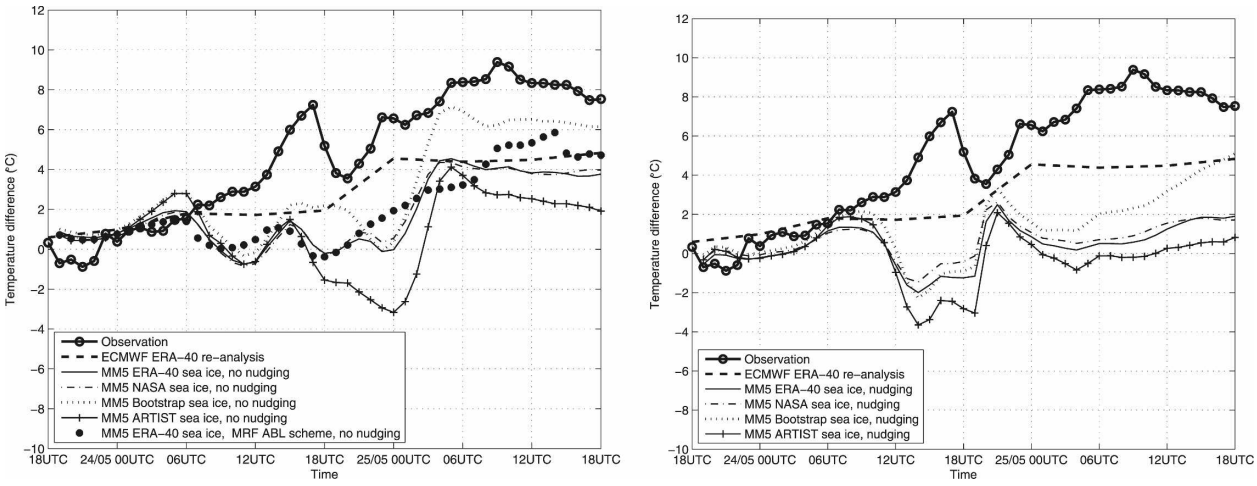

FIG. 6. Time series of air temperature difference between buoys 4 and 2; (left) experiments without nudging and (right) experiments with nudging.

est temperature differences: this is because it is good for buoy 4 but yields too-high temperatures for buoy 2, while ERA-40 and NASA Team sea ice concentrations yield systematically too-high temperatures for both buoys (Fig. 5). We should remind readers that these results are based only on a case study.

Temperature differences between the extreme results, based on bootstrap and NASA Team sea ice concentrations, are shown in Fig. 7. Differences in sea ice concentration and air temperature are clearly collocated. The maximum temperature difference at the end of the simulation period was 13°C. The air temperature does not, however, only depend on the local sea ice concentration but most importantly on the fetch. We estimated the cumulative fetch over open water for an air mass traveling from the southwest to the centroid of the buoy locations at the end of the simulation period. The estimation was based on calculation of (three-dimensional) backward trajectories (Fujinuma 2003) for time scales of 6, 12, 24, 48, and 84 h. On the basis of these trajectories, the air mass had left the northwestern corner of the Ronne Ice Shelf (75°S, 62°W) on 22

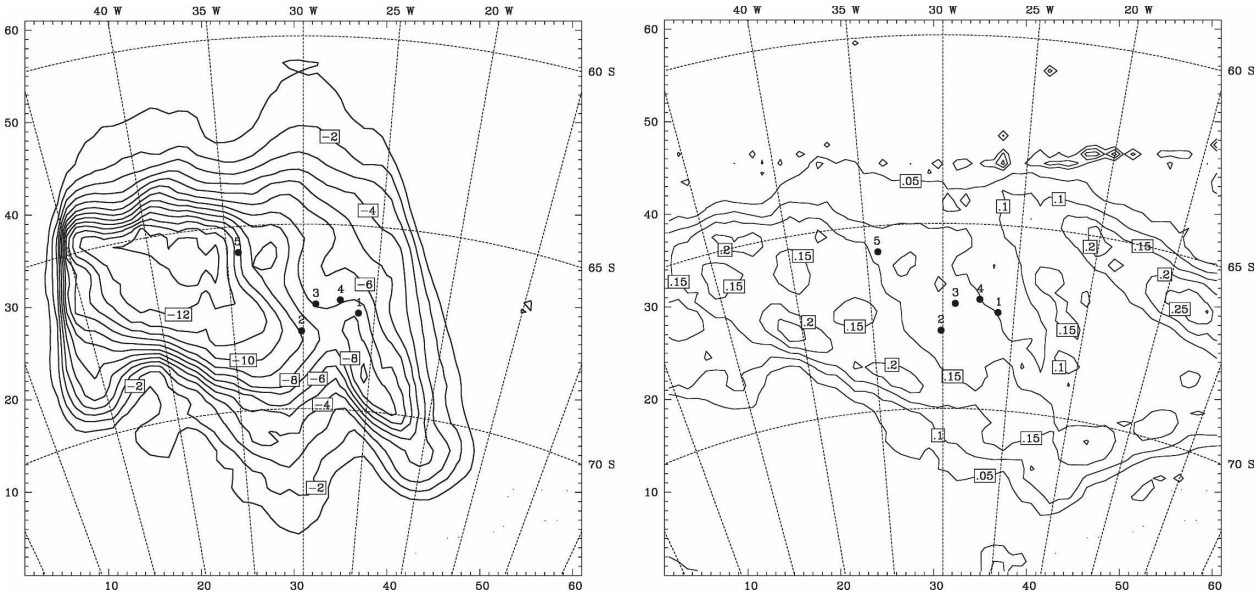

FIG. 7. Differences in (left) temperature and (right) sea ice concentration between simulations with bootstrap and NASA Team sea ice concentration. The situations are shown at the end of the 48-h simulations.

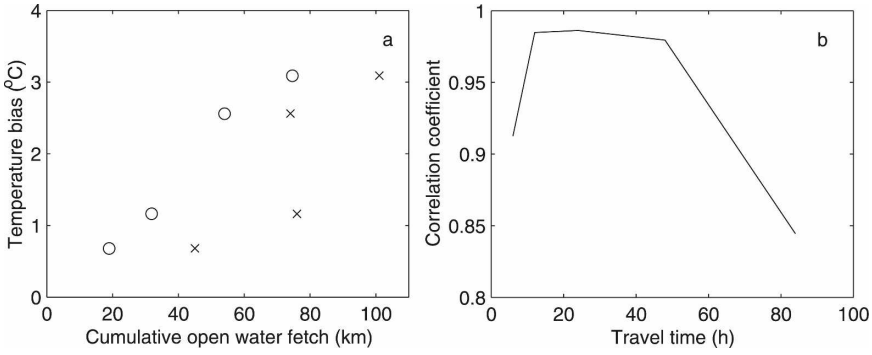

FIG. 8. (a) The air temperature bias from Table 3 (nudging) as a function of the cumulative open-water fetch calculated for a 24-h (circles) and 84-h (crosses) backward trajectory, and (b) the correlation coefficient between the air temperature bias and the time of the backward trajectory used to calculate the cumulative open-water fetch.

May 2000, at 0600 UTC. It then passed over sea ice, and the cumulative open-water fetch depended on the ice concentration dataset applied. In Fig. 8a we show the bias of the simulated air temperature (Table 3, results with nudging) as a function of the cumulative open-water fetch calculated for 24- and 84-h backward trajectories (for clarity, results for 6-, 12-, and 48-h trajectories are not shown). The correlation coefficient between the air temperature bias and the time span of the backward trajectory used is shown in Fig. 8b. It is evident that the bias is strongly related to the sea ice concentration field applied, and the bias at the buoy centroid seems to be most sensitive to the amount of open water that the air had been in contact with during the most recent 12–48 h. The differences between the correlation coefficients (ranging from 0.84 to 0.99) are, however, not statistically significant, but it seems that the amount of open water further back in the trajectory had less effect on the air temperature bias. This is illustrated by the 84-h calculation (Fig. 8a): almost identical open-water fetches of 74 and 76 km (based on ERA-40 and ARTIST sea ice concentrations, respectively) result in a very different bias.

Time series of the observed and modeled wind speed are shown in Fig. 9. Values from the lowest model level at 2 m have been adjusted to the observation level of 1 m by a logarithmic height correction. We only show results from buoy 2, since wind data from other buoys included long (more than 6 h) periods of zero or near-zero winds—probably because of ice accretion in the anemometers. Comparison with buoy 2 suggests that MM5 has a tendency to overestimate the 1-m wind speed. This may be related to errors in (a) the pressure gradient, (b) the surface roughness, and (c) the thermal

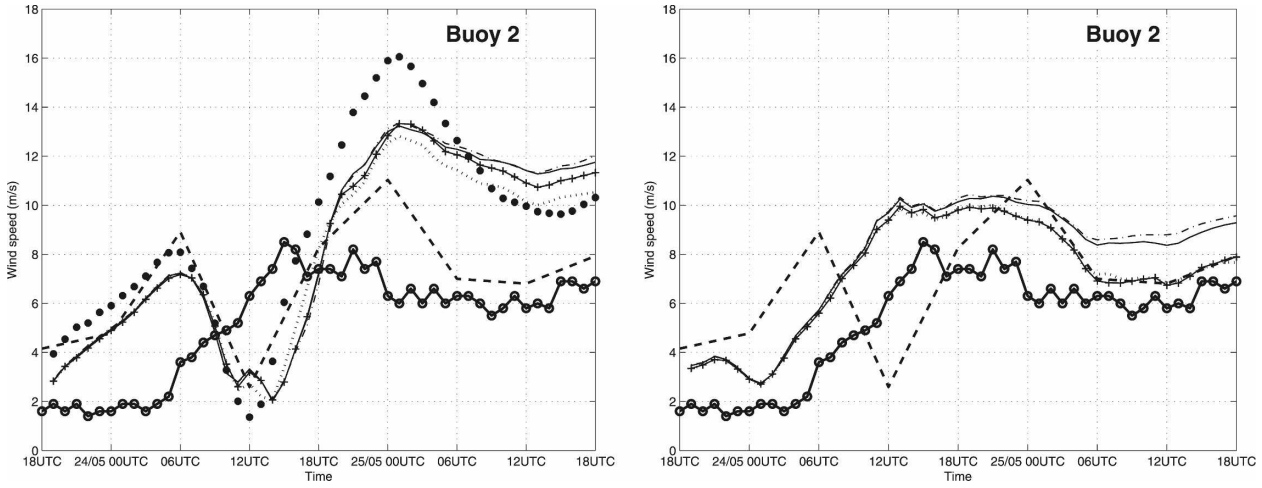

FIG. 9. Time series of the observed and modeled wind speed at buoy 2; (left) experiments without nudging and (right) experiments with nudging. Line types are as in Figs. 5 and 6.

stratification. As the buoy data were utilized in ERA-40, the pressure gradient in ERA-40 was free of large errors, and this was also the case in MM5 experiments with nudging. The overestimation still present in the experiments with nudging (Fig. 9) may have resulted from factors (b) and/or (c). The wind speed at 1-m height is sensitive to the aerodynamic roughness length (z_0) applied. In MM5, z_0 over sea ice is simply set to 0.001 m, while in reality it is affected by various factors including ice ridges, sastrugi, and freeboard of floe edges (Lüpkes and Birnbaum 2005), and z_0 over sea ice (excluding grease, nilas, and pancake ice) can range from 0.0003 to 0.1 m (Guest and Davidson 1991). Unfortunately we lack information on the actual z_0 in the study region.

To estimate the stability effect (c), we calculated the Richardson number (Ri) at the site of buoy 2 on the basis of each model experiment: the surface temperature as well as wind speed and air temperature at the lowest model level were applied. In the first day of simulations, with northerly winds, the differences in Ri between the experiments were minor, as were the differences in the wind speed between experiments applying nudging (Fig. 9). In the second day with southerly winds, the differences in the simulated wind speed grew and, in the experiments applying bootstrap and ARTIST sea ice concentrations, Ri was from -0.01 to 0.01, while the values ranged from -0.11 to -0.01 in the experiments applying NASA Team and ERA-40 sea ice concentrations. The differences in Ri between the experiments were mostly due to differences in the temperature profile. Accordingly, the experiments with lower sea ice concentration yielded more unstable surface layer, which tends to increase near-surface wind speeds through enhanced vertical mixing of momentum.

Higher in the ABL the air temperatures were still sensitive to the sea ice concentration data applied: differences up to 10°C between experiments 1 (ERA-40 sea ice) and 3 (bootstrap sea ice) reached the height of 50 m, differences up to 8°C reached 100 m, and differences up to 3°C were still detected at heights above 200 m. Above the ABL, which extended up to 200–300 m depending on the ice concentration data applied, the simulated wind and temperature fields were not greatly affected by the sea ice concentration. This indicates that the disturbances generated by heating from leads did not penetrate through the top of the ABL. On the other hand, cross sections up to the height of 2 km strongly depended on the ABL scheme applied in Polar MM5. Figure 10 therefore displays results from experiments 1 and 5, applying the ERA-40 sea ice concentration with Eta and MRF ABL schemes, respectively. The Eta scheme shows a strong low-level jet (LLJ) at the end of the simulation period, with a core at 750-m height. The LLJ was a result of baroclinicity: the temperature increased toward the east, with warm air to the right of the wind vector. Hence, according to the thermal wind law, the geostrophic wind decreased with height (in the Southern Hemisphere). In the ABL, the wind speed was reduced by the surface friction, and an LLJ was therefore generated. The fine structure of the wind field below the LLJ core in the layer from 300 to 750 m was also in accordance with the temperature distribution. Applying the MRF scheme (Fig. 10, right panel), the mixed layer became much deeper. Maximum wind speed in the LLJ core was only 15 m s^{-1} instead of 21 m s^{-1} produced by the Eta scheme.

c. Cloud cover

The cloud cover was qualitatively similar in experiments applying Eta and MRF schemes. At the end of the simulation period, when the temperature differences between the experiments were largest, all buoys were under a thin cloud cover (vertically integrated cloud water less than 0.01 kg m^{-2}). This suggests that the large temperature differences (Fig. 10) resulted more or less directly from the different turbulent flux fields without major feedback effects from cloud radiative forcing. The difference in the vertically integrated cloud water between simulations applying NASA Team and bootstrap sea ice concentrations ranged from -0.02 to 0.006 kg m^{-2}, but the typical absolute values of the difference were less than 0.001 kg m^{-2}, which was of the order of 10% as a relative difference.

d. Turbulent surface fluxes

Sea ice concentration has a strong influence on turbulent surface fluxes. In Fig. 11, we show the fields of sensible and latent heat flux at the end of the simulation period, based on the following MM5 experiments: 1 (ERA-40 sea ice concentration applying Eta ABL scheme), 3 (bootstrap sea ice concentration, Eta scheme), and 5 (ERA-40 sea ice concentration, MRW ABL scheme). The surface fluxes were not particularly sensitive to the ABL scheme used but were very sensitive to the sea ice concentration data: the results of the two model experiments (1 and 5) with ERA-40 sea ice concentration but different ABL scheme were qualitatively similar, but results from the experiment with bootstrap sea ice concentration were clearly different (Fig. 11). The bootstrap-based results, with the most compact ice cover, included large areas with stable stratification and downward sensible heat flux, while results using ERA-40 sea ice concentration show down-

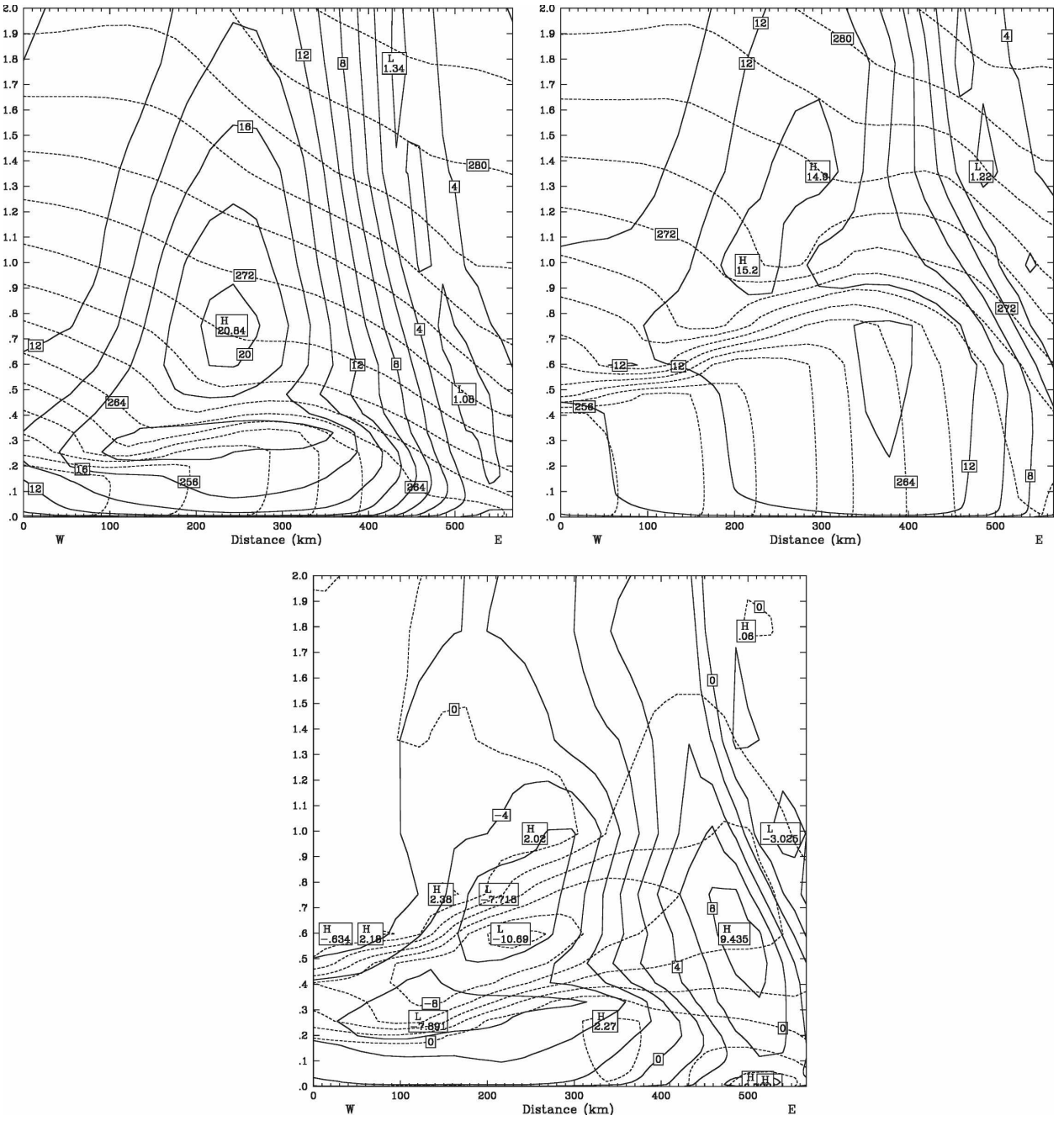

FIG. 10. Cross section of temperature (dashed lines) and wind speed (solid lines) at the end of the 48-h simulation period. (top left) Experiment 1 (ERA-40 sea ice concentration, Eta ABL scheme); (top right) experiment 5 (ERA-40 sea ice concentration, MRF ABL scheme). (bottom) The difference in the air temperature and wind speed between experiments 1 and 5.

ward fluxes restricted to the southeastern part of domain 2. On the other hand, the largest upward fluxes were produced in the bootstrap-based experiments: the air was coldest in these experiments, and when the cold air was advected over regions with less than 90% ice concentration—in the middle and northern parts of domain 2—the local fluxes were larger than in the experiments yielding warmer ABL. The fields of latent heat flux (Fig. 11, lower panel) were qualitatively similar to those of the sensible heat flux, but flux magnitudes were smaller and in some regions of downward sensible heat flux the latent heat flux was positive (e.g., southeastern parts of domain 2 in experiment 5). Using buoy data and a thermodynamic snow–ice model, Vihma et

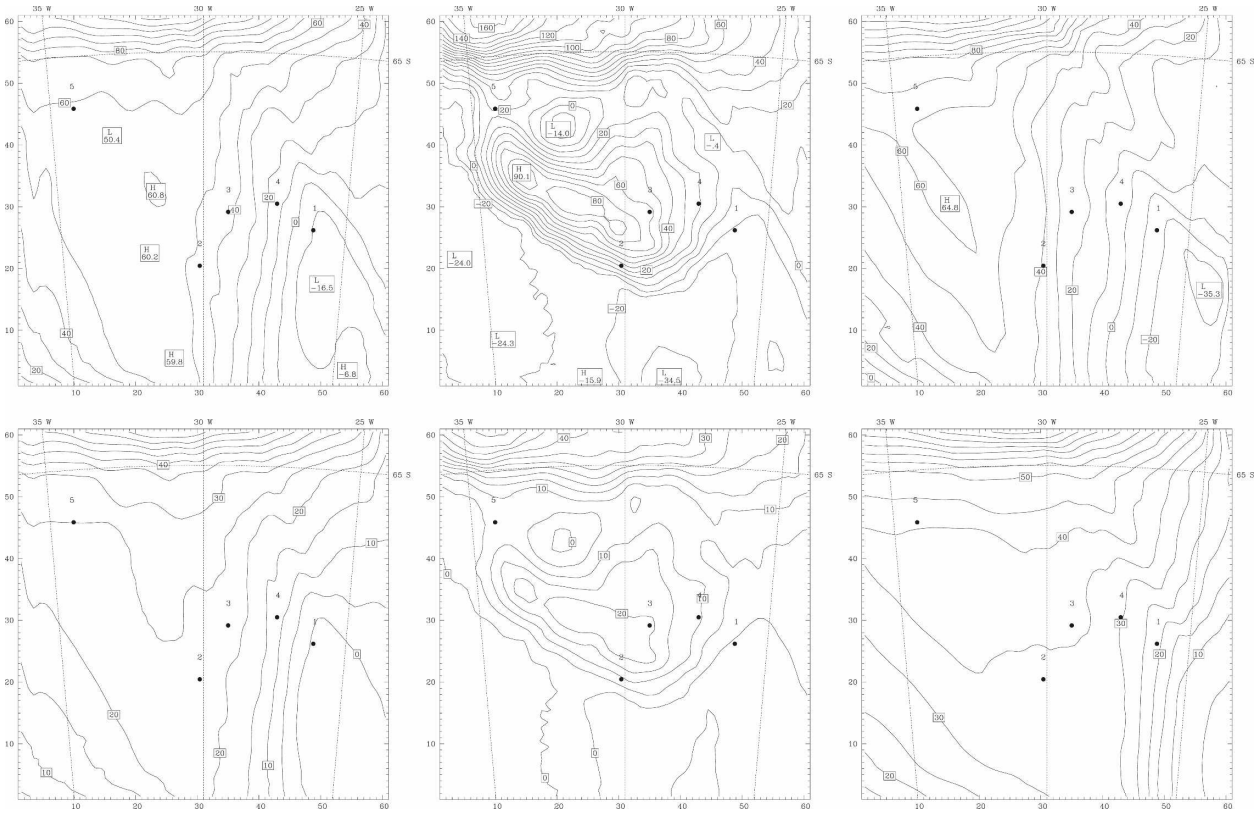

FIG. 11. Turbulent surface fluxes of (top) sensible heat and (bottom) latent heat at the end of the 48-h simulation period based on experiments (left) 1 (ERA-40 sea ice, Eta scheme), (middle) 3 (bootstrap sea ice, Eta scheme), and (right) 5 (ERA-40 sea ice, MRF scheme).

al. (2002) calculated that the area-averaged sensible heat fluxes were downward and latent heat fluxes upward for all seasons in the Weddell Sea. The results from our 48-h mesoscale simulation cannot be used as a basis for conclusions on larger spatial and temporal scales, such as these, but they support the observation that over sea ice the surface sensible and latent heat fluxes sometimes have the opposite sign.

6. Discussion

Our results on the sensitivity of the ABL to sea ice concentration can be compared with previous studies. In a climate-scale modeling study, Lachlan-Cope (2005) found that the sensitivity of near-surface air temperature to Antarctic sea ice concentration varies spatially, our study region representing low sensitivity compared to regions to the west of the Antarctic Peninsula. Simmonds and Budd (1991) demonstrated that the large-scale circulation in the Southern Hemisphere is sensitive to leads. Their simulation strategy was very different, however: 600-day simulations were made applying a general circulation model with the open-water fraction in the sea ice zone set to 5%, 50%, 80%, and 100%. To compare the present study against mesoscale studies with the range of variability in the sea ice concentration close to the uncertainty of the available remote sensing data, we have to look at experiments in the Arctic and the Baltic Sea.

Vihma and Brümmer (2002) studied a winter cold-air outbreak in the Baltic Sea: the area of aircraft observations included a 50-km-long fetch over fractured ice with 30% open-water fraction. Ignoring the open water in a model sensitivity experiment only resulted in approximately 1°C reduction in the temperature of a 300-m-high mixed layer. In Vihma et al. (2005), the fetch over leads in the Arctic sea ice zone was small (5% open-water fraction over an area 30 km wide), and model sensitivity tests with and without leads did not show any detectable effects on the 40-m air temperature, although the effects on the surface temperature and turbulent heat flues were large. Introducing the ARTIST sea ice algorithm, Kaleschke et al. (2001) presented sensitivity studies for different flow conditions in the Arctic in March 1998. During an off-ice flow perpendicular to the ice edge, the influence of the ice con-

centration data (ARTIST and NASA Team) on the temperature of a 300-m-high mixed layer was only 0.5°C. The differences in the ice concentration occurred over a fetch of 40 km. Drusch (2006) applied the ECMWF model in experiments over the Baltic Sea for a 2-month-long winter period. The sea ice concentration was based either on the global NCEP dataset with a 0.5° spatial resolution, applied operationally in the ECMWF, or on a dataset by the Swedish Meteorological and Hydrological Institute with 1-km resolution. The experiments revealed large differences in the spatially aggregated turbulent surface fluxes, which generated differences in the ABL height and temperatures. The maximum differences in near-surface air temperature were approximately 3°C. Accordingly, compared to our study, relatively small differences in the air temperature have been simulated in previous studies with the difference in the sea ice concentration occurring over shorter fetches.

Kaleschke et al. (2001), however, also included a case of a flow parallel to the ice edge, and a maximum difference of 6°C in the modeled 40-m air temperature was reached between the experiments applying ARTIST and NASA Team ice concentration data. The significant temperature difference was probably due to the strong horizontal air temperature gradient that was generated over the ice edge during the parallel flow. The ice concentration controlled the simulated location and strength of this gradient. Both flow conditions of Kaleschke et al. (2001) showed the ARTIST algorithm to give better results, validated against aircraft observations, in a similar manner to the present investigation.

Two studies (Andersson and Gustafsson 1994; Gustafsson et al. 1998), applying the operational weather forecasting High-Resolution Limited-Area Model (HIRLAM) and addressing easterly cold-air outbreaks over the Baltic Sea, have demonstrated that accurate information on the sea ice border is essential for the forecasting of convective snowfall. The local surface type had a large effect on the turbulent surface fluxes and on the initial development of convective snowbands. Effects of sea ice concentration on the cloud cover have also been detected by Drusch (2006) and Monaghan et al. (2005), but quantitative comparisons against our study are difficult due to different simulation strategies and measures for the cloud cover.

The simulated wind field included a strong low-level jet, which was sensitive to the ABL scheme applied, but was produced both by Eta and MRF schemes. Low-level jets related to inertial oscillations have been observed over the Weddell Sea ice cover (Andreas et al. 2000). The LLJ was generated when a stable stratification was reestablished after a storm: the synoptic-scale change in stratification acted analogously to a diurnal change for the generation of the classical nocturnal LLJ. In our case, in the buoy region with lower sea ice concentration, the stratification was predominantly unstable and the LLJ was generated by baroclinicity. LLJs related to baroclinicity have previously been observed over the ice edge zone, where a temperature gradient prevails between the marine and polar air masses (e.g., Drüe and Heinemann 2001). In such cases, the LLJs are usually oriented parallel to the ice edge. In our case, the LLJ occurred 300–400 km south of the ice edge, and was oriented perpendicular to it. It is noteworthy that nearby our study area mesoscale cyclogenesis is active (Carrasco et al. 2003), and it often arises from baroclinic processes associated with boundary layer fronts.

7. Conclusions

We have presented the first mesoscale meteorological modeling experiments for the Antarctic sea ice zone with detailed validation at mesoscale spatial resolution. The success of Polar MM5 in reproducing the observed atmospheric pressure and near-surface air temperature fields strongly depended on the lower boundary conditions. The differences in sea ice concentration based on four satellite algorithms were large, though there was no direct method to validate the ice concentration datasets. Validation results have been presented in the literature (e.g., Agnew and Howell 2003), but the success of a particular satellite algorithm also depends strongly on the ice conditions: a good algorithm for multiyear Arctic sea ice is not necessarily suited to the generally thinner and less compact Antarctic sea ice. The sensitivity of our model results to sea ice concentration was, however, so large that we suggest that the model results can give indirect information on the validity of the ice concentration datasets. This case study for the Antarctic sea ice zone in late autumn demonstrated that the bootstrap and ARTIST algorithms were more accurate than the NASA Team algorithm and the method applied in ERA-40.

Compact sea ice fields with more than 90% ice concentration are particularly difficult to determine accurately by satellite methods, especially when accounting for areas of new, thin ice. Dividing the surface simply into two types, sea ice and open water, is an oversimplification (Schröder et al. 2003), since the surface temperature of thin, new ice is between that of thick ice and open water. This is not taken into account in the parameterization of surface fluxes by the mosaic method. Several ice types could be easily included in the mosaic method, but are not beneficial without detailed satel-

lite-based information on their areal coverage. Another approach would be the Ensemble Prediction System (EPS; Tracton and Kalnay (1993)). Instead of, or in addition to, perturbing the initial conditions, as traditionally in EPS, the lower boundary conditions could be perturbed within the range of uncertainty in the ice concentration.

The effects of nudging were variable: the pressure fields and (for buoy 2) the wind field were improved, but the near-surface temperatures were not much affected. Applying the bootstrap ice concentration data nudging made the temperature fields worse (Table 3; Fig. 6). Also, previous studies applying MM5 have demonstrated that analysis nudging (nudging the model solutions toward gridded analyses instead of directly toward individual observations) can have detrimental effects (Deng and Stauffer 2006).

The cumulative fetch over open water correlated with the bias of the modeled air temperature, with the highest correlation for time scales of 12 to 48 h. Compared to previous studies, the modeled air temperatures were more sensitive to sea ice concentration because the cumulative open-water fetches were longer. The sea ice concentration data affected the simulated air temperature in the atmospheric boundary layer, but above it the temperature and wind fields were more strongly controlled by the boundary layer scheme applied in Polar MM5. The MRF scheme generated a deeper ABL than the Eta scheme. Deng and Stauffer (2006) and Tombrou et al. (2007) observed that the MRF scheme in MM5 has a tendency to overestimate the ABL height. In our study, the near-surface temperatures based on the MRF scheme did not compare as well to the buoy data as the simulations using the Eta scheme.

We stress that although the different simulation strategies (with respect to nudging and ABL scheme) yielded different results and each had their own strengths and weaknesses, they were all very sensitive to sea ice concentration; the largest differences in 2-m air temperature reaching 13°C solely due to this factor. Finally, it should be noted that from the point of view of meteorological modeling, it is not enough that the sea concentration is based on an accurate remote sensing algorithm, but the boundary conditions should also be updated frequently enough. For forecast applications, it would therefore be essential to base the boundary conditions on a sea ice model, as done, for example, in Dierer et al. (2005).

Acknowledgments. We thank David Bromwich, Andrew Monaghan, Lorenzo Claveri, and Erik Gregow for valuable advice in running MM5, and Hannu Savijärvi for fruitful discussions. Lars Kaleschke (University of Hamburg), the National Snow and Ice Data Center, and the ECMWF are acknowledged for providing us with sea ice and atmospheric reanalysis data. This study was supported by the Academy of Finland Grant 210794. We are grateful to the Alfred Wegener Institut für Polar- und Meeresforschung, Bremerhaven, for the opportunity to work from F/S *Polarstern* during the field experiment and thank the captain and crew for their kind cooperation.

REFERENCES

Adams, N., 2005: Identifying the characteristics of strong southerly wind events at Casey station in East Antarctica using a numerical weather prediction system. *Mon. Wea. Rev.,* **133,** 3548–3561.

Agnew, T., and S. Howell, 2003: The use of operational ice charts for evaluating passive microwave ice concentration data. *Atmos.–Ocean,* **41,** 317–331.

Alam, A., and J. A. Curry, 1997: Determination of surface turbulent fluxes over leads in Arctic sea ice. *J. Geophys. Res.,* **102,** 3331–3344.

Andersson, T., and N. Gustafsson, 1994: Coast of departure and coast of arrival: Two important concepts for the formation and structure of convective snowbands over seas and lakes. *Mon. Wea. Rev.,* **122,** 1036–1049.

Andreas, E. L, 1985: Heat and moisture advection over Antarctic sea ice. *Mon. Wea. Rev.,* **113,** 736–746.

——, and B. A. Cash, 1999: Convective transfer over wintertime leads and polynyas. *J. Geophys. Res.,* **104,** 25 721–25 734.

——, C. A. Paulson, R. M. Williams, R. W. Lindsay, and J. A. Businger, 1979: The turbulent heat flux from Arctic leads. *Bound.-Layer Meteor.,* **17,** 57–91.

——, K. J. Claffey, and A. P. Makshtas, 2000: Low-level atmospheric jets and inversions over the western Weddell Sea. *Bound.-Layer Meteor.,* **97,** 459–486.

——, R. E. Jordan, and A. P. Makshtas, 2004: Simulations of snow, ice, and near-surface atmospheric processes on Ice Station Weddell. *J. Hydrometeor.,* **5,** 611–624.

Bareiss, J., 2008: ISPOL weather conditions in the context of long-term climate variability in the northwestern Weddell Sea. *Deep-Sea Res.,* in press.

Bennet, T. J., and K. Hunkins, 1986: Atmospheric boundary layer modification in the marginal ice zone. *J. Geophys. Res.,* **91,** 13 033–13 044.

Birnbaum, G., 2003: Simulation of the atmospheric circulation in the Weddell Sea region using the limited-area model REMO. *Theor. Appl. Climatol.,* **74,** 255–271.

Bromwich, D. H., J. J. Cassano, T. Klein, G. Heinemann, K. M. Hines, K. Steffen, and J. E. Box, 2001: Mesoscale modeling of katabatic winds over Greenland with the Polar MM5. *Mon. Wea. Rev.,* **129,** 2290–2309.

——, A. J. Monaghan, J. G. Powers, J. J. Cassano, H. Wei, Y. Kuo, and A. Pellegrini, 2003: Antarctic Mesoscale Prediction System (AMPS): A case study from the 2000–01 field season. *Mon. Wea. Rev.,* **131,** 412–434.

——, ——, K. W. Manning, and J. G. Powers, 2005: Real-time forecasting for the Antarctic: An evaluation of the Antarctic Mesoscale Prediction System (AMPS). *Mon. Wea. Rev.,* **133,** 579–603.

Carrasco, J. F., D. H. Bromwich, and A. J. Monaghan, 2003: Distribution and characteristics of mesoscale cyclones in the Antarctic: Ross Sea east to the Weddell Sea. *Mon. Wea. Rev.,* **131,** 289–301.

Cassano, J. J., J. E. Box, D. H. Bromwich, L. Li, and K. Steffen, 2001: Evaluation of Polar MM5 simulations of Greenland's atmospheric circulation. *J. Geophys. Res.,* **106,** 33 867–33 889.

Cavalieri, D., C. Parkinson, P. Gloersen, and H. J. Zwally, cited 2006: Sea ice concentrations from *Nimbus-7* SSMR and DMSP SSM/I passive microwave data. National Snow and Ice Data Center, Boulder, CO, digital media. [Available online at http://www.nsidc.com/data/.]

Claussen, M., 1990: Area-averaging of surface fluxes in a neutrally stratified, horizontally inhomogeneous atmospheric boundary layer. *Atmos. Environ.,* **24A,** 1349–1360.

Comiso, J. C., 1986: Characteristics of Arctic winter sea ice from satellite multispectral microwave observations. *J. Geophys. Res.,* **91,** 975–994.

——, cited 2006: DMSP SSM/I daily and monthly polar gridded sea ice concentrations, May 2000. J. Maslanik and J. Stroeve, Eds., National Snow and Ice Data Center, Boulder, CO, digital media. [Available online at http://www.nsidc.com/data/.]

——, and C. W. Sullivan, 1986: Satellite microwave and in-situ observations of the Weddell Sea ice cover and its marginal ice zone. *J. Geophys. Res.,* **91,** 9663–9681.

Dare, R. A., and B. W. Atkinson, 1999: Numerical modeling of atmospheric response to polynyas in the Southern Ocean sea ice zone. *J. Geophys. Res.,* **104,** 16 691–16 708.

Deng, A., and D. R. Stauffer, 2006: On improving 4-km mesoscale model simulations. *J. Appl. Meteor. Climatol.,* **45,** 361–381.

Dierer, S., K. H. Schlünzen, G. Birnbaum, B. Brümmer, and G. Müller, 2005: Atmosphere–sea ice interactions during a cyclone passage investigated by using model simulations and measurements. *Mon. Wea. Rev.,* **133,** 3678–3692.

Doble, M. J., and P. Wadhams, 2006: Dynamical contrasts between pancake and pack ice, investigated with a drifting buoy array. *J. Geophys. Res.,* **111,** C11S24, doi:10.1029/2005JC003320.

——, M. D. Coon, and P. Wadhams, 2003: Pancake ice formation in the Weddell Sea. *J. Geophys. Res.,* **108,** 3209, doi:10.1029/2002JC001373.

Drüe, C., and G. Heinemann, 2001: Airborne investigation of Arctic boundary-layer fronts over the marginal ice zone of the Davis Strait. *Bound.-Layer Meteor.,* **101,** 261–292.

Drusch, M., 2006: Sea ice concentration analyses for the Baltic Sea and their impact on numerical weather prediction. *J. Appl. Meteor. Climatol.,* **45,** 982–994.

Dudhia, J., D. Gill, K. Manning, W. Wang, and C. Bruyere, cited 2005: PSU/NCAR Mesoscale Modeling System, tutorial class notes and user's guide, MM5 Modeling System Version 3. Mesoscale and Microscale Meteorology Division, National Center for Atmospheric Research. [Available online at http://www.mmm.ucar.edu/mm5/documents/.]

Fiorino, M., cited 2007: A multi-decadal daily sea-surface temperature and sea-ice concentration data set for the ERA-40 reanalysis. European Centre for Medium-Range Weather Forecasts, Shinfield, Reading, United Kingdom. [Available online at http://www.ecmwf.int/publications.]

Fujinuma, Y., 2003: Data analysis and graphic display system for atmospheric research using PC. GCER Rep. M014-2003, Center for Global Environmental Research and National Institute for Environmental Studies, Japan, 240 pp.

Grell, G. A., J. Dudhia, and D. R. Stauffer, 1994: A description of the fifth-generation Penn State/NCAR Mesoscale Model (MM5). NCAR Tech. Rep. NCAR/TN-398+STR, 122 pp.

Guest, P. S., and K. L. Davidson, 1991: The aerodynamic roughness of different types of sea ice. *J. Geophys. Res.,* **96,** 4709–4721.

Guo, Z., D. H. Bromwich, and J. J. Cassano, 2003: Evaluation of Polar MM5 simulations of Antarctic atmospheric circulation. *Mon. Wea. Rev.,* **131,** 384–411.

Gustafsson, N., L. Nyberg, and A. Omstedt, 1998: Coupling of a high-resolution atmospheric model and an ocean model for the Baltic Sea. *Mon. Wea. Rev.,* **126,** 2822–2846.

Hack, J. J., B. A. Boville, B. P. Briegleb, J. T. Kiehl, P. J. Rasch, and D. L. Williamson, 1993: Description of the NCAR community climate model (CCM2). NCAR Tech. Rep. NCAR/TN-382+STR, 108 pp.

Hong, S. Y., and H. L. Pan, 1996: Nonlocal boundary layer vertical diffusion in a medium range forecast model. *Mon. Wea. Rev.,* **124,** 2322–2339.

Inoue, J., M. Kawashima, Y. Fujiyoshi, and M. Wakatsuchi, 2005: Aircraft observations of air-mass modification over the Sea of Okhotsk during sea ice growth. *Bound.-Layer Meteor.,* **117,** 111–129.

Janjic, Z. I., 1994: The step-mountain eta coordinate model: Further developments of the convection, viscous sublayer, and turbulence closure schemes. *Mon. Wea. Rev.,* **122,** 927–945.

Kaleschke, L., C. Lüpkes, T. Vihma, J. Haarpaintner, A. Bochert, J. Hartmann, and G. Heygster, 2001: SSM/I sea ice remote sensing for mesoscale ocean-atmosphere interaction analysis. *Can. J. Remote Sens.,* **27,** 526–537.

Kern, S., L. Kaleschke, and D. Clausi, 2003: A comparison of two 85-GHz SSM/I ice concentration algorithms with AVHRR and ERS-2 SAR imagery. *IEEE Trans. Geosci. Remote Sens.,* **41,** 2294–2306.

Kottmeier, C., and L. Sellman, 1996: Atmospheric and oceanic forcing of Weddell Sea ice motion. *J. Geophys. Res.,* **101,** 20 809–20 824.

Lachlan-Cope, T., 2005: Role of sea ice in forcing the winter climate of Antarctica in a global climate model. *J. Geophys. Res.,* **110,** D03110, doi:10.1029/2004JD004935.

Lüpkes, C., and G. Birnbaum, 2005: Surface drag in the Arctic marginal sea-ice zone: A comparison of different parameterisation concepts. *Bound.-Layer Meteor.,* **117,** 179–211.

Mauritsen, T., G. Svensson, and B. Grisogono, 2005: Wave flow simulations over Arctic leads. *Bound.-Layer Meteor.,* **117,** 259–273.

Monaghan, A. J., D. H. Bromwich, H. Wei, A. M. Cayette, J. G. Powers, Y. Kuo, and M. A. Lazzara, 2003: Performance of weather forecast models in the rescue of Dr. Ronald Shemenski from the South Pole in April 2001. *Wea. Forecasting,* **18,** 142–160.

——, ——, J. G. Powers, and K. W. Mannigan, 2005: The climate of the McMurdo, Antarctica, region as represented by one year of forecasts from the Antarctic Mesoscale Prediction System. *J. Climate,* **18,** 1174–1189.

Parish, T. R., and G. Wendler, 1991: The katabatic wind regime at Adelie Land, Antarctica. *Int. J. Climatol.,* **11,** 97–107.

——, and R. Walker, 2006: A re-examination of the winds of Adélie Land, Antarctica. *Aust. Meteor. Mag.,* **55,** 105–117.

Parkinson, C. L., 2004: Southern Ocean sea ice and its wider linkages: Insights revealed from models and observations. *Antarct. Sci.,* **16,** 387–400.

Pinto, J. O., A. Alam, J. A. Maslanic, J. A. Curry, and R. S. Stone, 2003: Surface characteristics and atmospheric footprint of

springtime Arctic leads at SHEBA. *J. Geophys. Res.,* **108,** 8051, doi:10.1029/2000JC000473.

Reisner, J., R. M. Rasmussen, and R. T. Bruintjes, 1998: Explicit forecasting of supercooled liquid water in winter storms using the MM5 mesoscale model. *Quart. J. Roy. Meteor. Soc.,* **124,** 1071–1107.

Renfrew, I. A., and J. C. King, 2000: A simple model of the convective internal boundary layer and its application to surface heat flux estimates within polynyas. *Bound.-Layer Meteor.,* **94,** 335–356.

——, ——, and T. Markus, 2002: Coastal polynyas in the southern Weddell Sea: Variability of the surface energy budget. *J. Geophys. Res.,* **107,** 3063, doi:10.1029/2000JC000720.

Schröder, D., T. Vihma, A. Kerber, and B. Brümmer, 2003: On the parameterization of turbulent surface fluxes over heterogeneous sea ice surfaces. *J. Geophys. Res.,* **108,** 3195, doi:10.1029/2002JC001385.

Simmonds, I., and W. Budd, 1991: Sensitivity of the Southern Hemisphere circulation to leads in the Antarctic pack ice. *Quart. J. Roy. Meteor. Soc.,* **117,** 1003–1024.

——, A. Rafter, T. Cowan, A. B. Watkins, and K. Keay, 2005: Large-scale vertical momentum, kinetic energy and moisture fluxes in the Antarctic sea-ice region. *Bound.-Layer Meteor.,* **117,** 149–177.

Swift, C. T., and D. J. Cavalieri, 1985: Passive microwave remote sensing for sea ice research. *Earth Observ. Syst.,* **66,** 1210–1212.

Tombrou, M., A. Dandou, C. Helmis, E. Akylas, G. Angelopoulos, H. Flocas, V. Assimakopoulos, and N. Soulakellis, 2007: Model evaluation of the atmospheric boundary layer and mixed-layer evolution. *Bound.-Layer Meteor.,* **124,** 61–79.

Tracton, M. S., and E. Kalnay, 1993: Operational ensemble prediction at the National Meteorological Center: Practical aspects. *Wea. Forecasting,* **8,** 379–398.

Uppala, S. M., and Coauthors, 2005: The ERA-40 Re-analysis. *Quart. J. Roy. Meteor. Soc.,* **131,** 2961–3012.

Vihma, T., 1995: Subgrid parameterization of surface heat and momentum fluxes over polar oceans. *J. Geophys. Res.,* **100,** 22 625–22 646.

——, and B. Brümmer, 2002: Observations and modelling of the on-ice and off-ice air flow over the northern Baltic Sea. *Bound.-Layer Meteor.,* **103,** 1–27.

——, J. Uotila, B. Cheng, and J. Launiainen, 2002: Surface heat budget over the Weddell Sea: Buoy results and model comparisons. *J. Geophys. Res.,* **107,** 3013, doi:10.1029/2000JC000372.

——, C. Lüpkes, J. Hartmann, and H. Savijärvi, 2005: Observations and modelling of cold-air advection over Arctic sea ice. *Bound.-Layer Meteor.,* **117,** 275–300.

Wassermann, S., C. Schmitt, C. Kottmeier, and I. Simmonds, 2006: Coincident vortices in Antarctic wind fields and sea ice motion. *Geophys. Res. Lett.,* **33,** L15810, doi:10.1029/2006GL026005.

Watkins, A. B., and I. Simmonds, 1995: Sensitivity of numerical prognoses to Antarctic sea ice distribution. *J. Geophys. Res.,* **100,** 22 681–22 696.

——, and ——, 1998: Relationships between Antarctic sea-ice concentration, wind stress and temperature temporal variability, and their changes with distance from the coast. *Ann. Glaciol.,* **27,** 409–412.

Wendler, G., B. Hartmann, C. Wyatt, M. Shulski, and H. Stone, 2005: Midsummer energy balance for the southern seas. *Bound.-Layer Meteor.,* **117,** 131–148.

Yen, Y. C., 1981: Review of thermal properties of snow, ice and sea ice. CRREL Rep. 81-10, Cold Regions Research and Engineering Laboratory, Hanover, NH, 27 pp.